J. Fluid Mech. (1966), *vol.* 25, *part* 2, *pp.* 299–320
Printed in Great Britain

Velocity and temperature profiles in adverse pressure gradient turbulent boundary layers

By A. E. PERRY, J. B. BELL AND P. N. JOUBERT
Department of Mechanical Engineering, University of Melbourne

(Received 27 September 1965)

A correlation scheme for velocity and temperature profiles is derived for turbulent boundary layers in adverse pressure gradients. The resulting analytical expressions are obtained by what could be referred to as 'regional similarity' arguments. This avoids the need to make use of the Reynolds analogy (explicitly, at least) or the usual local gradient-type diffusion expressions for momentum and thermal transport ('the local similarity' and Boussinesq concept). The expressions agree well with experimental data for the velocity profiles and encouraging correlation is shown for the temperature profiles. The expressions cover a wider part of the profile than given by the logarithmic law of the wall. Surface roughness and Prandtl-number effects are included in the analysis.

1. Introduction

The local Stanton number along the surface of a hot or cold body of arbitrary shape with an attached turbulent boundary layer is determined by a solution of the mean thermal transport equation. This requires the velocity field (boundary layer and local skin-friction coefficients) to be known. Also some relationship between the temperature field (the thermal boundary layer) and velocity field is needed. The eddy viscosity distribution is known (since the velocity field is assumed to be known) and from this a corresponding thermal diffusivity coefficient is calculated. This is usually done using a form of the Reynolds analogy where the two transport coefficients are taken to be equal or else proportional to one another. This is essentially the basis of the Spalding analysis (Spalding 1961) which is now being widely applied.

Although the above methods of analysis are traditional, the concepts involved are quite often seriously questioned in the literature. In recent work by Rotta (1964) a more complex relationship between the two transport coefficients had to be used for correlating the velocity and temperature profiles in the outer regions of the boundary layer. Also, in a rather comprehensive review of the problem by Kestin & Richardson (1963) it is indicated that the concept of the various forms of the Reynolds analogy is still open to question.

Aside from the assumptions involved, the Spalding analysis is mathematically exact and appears adequate for many flow cases such as those with zero and favourable pressure gradients. However, it uses a simplified expression for the velocity field (a 'law of the wall' for the whole boundary-layer thickness) which makes it inapplicable to boundary layers in adverse pressure gradients.

Also the analysis cannot be used if predictions of skin friction cannot be made. Present methods for doing this are unreliable.

It can be seen that the state of knowledge of turbulent boundary-layer convection is rather incomplete and this is even more so for the adverse-pressure-gradient case.

This paper covers work which is aimed at the following:

(*a*) To attempt to find an expression for velocity profiles in turbulent boundary layers in adverse pressure gradients by similarity arguments rather than being committed to postulating a detailed model for the mechanism of turbulence. Such a model is exemplified by the Prandtl mixing-length hypothesis or the various other eddy viscosity models. It is hoped that the correlations obtained will lead the way to more reliable predictions of local skin-friction coefficients.

(*b*) To obtain expressions for the corresponding temperature profiles without having to rely on the dubious Reynolds analogy and thermal diffusivity concepts.

Because of the lack of any reliable detailed knowledge of the turbulent process, the appeal of physical arguments in similarity analyses is a rather subjective matter. For this reason the authors prefer to regard what follows as merely a tentative empirical description of the behaviour of the turbulent boundary layer. The assumed behaviour will be stated and certain analytical deductions will be made. The correctness of the description will be left entirely to present and future experimental verification. Some physical inferences about the results could be made, but these will not be used for supporting the analysis.

As with Millikan's work (Millikan 1938), the formal nature of the analysis has involved 'some sacrifice in the attention paid to the fundamental, elementary physical processes occurring'.† However, it is hoped that the analysis developed here will form an acceptable framework to which other more detailed theoretical and experimental investigations can be fitted.

Experimental data from a variety of sources appear to confirm the correlation scheme obtained in (*a*), and some recent experiments carried out at the University of Melbourne show encouraging results for part (*b*).

Parts of the velocity field analysis have been done elsewhere, and the various sources are indicated at the end of the analysis.

2. Analysis of velocity field

Assumptions

A turbulent boundary layer may be divided into a number of distinct regions when it develops over a surface along which the static pressure is rising. These regions are shown in figure 1.

Two major regions are the 'historical region' and 'wall region.' In the wall region, only the local variables govern the mean velocity profile. Such variables are shown in the following equation.

$$U = f(\tau_0, \alpha, \rho, \nu, y), \tag{1}$$

where U = mean velocity, τ_0 = local wall shear stress, α = local kinematic pressure gradient ($= (1/\rho)\, dp/dx$, where p is the static pressure), ρ = fluid density, ν = kinematic viscosity, y = distance from the wall.

† Quoting Millikan.

Higher derivatives of τ_0 and α may be involved but the above equation will be regarded valid for a wall region restricted to sufficiently small values of y.

In the historical region, upstream events have an influence on the mean velocity profile.

In the wall region, the following three subregions will be assumed to exist (see figure 1).

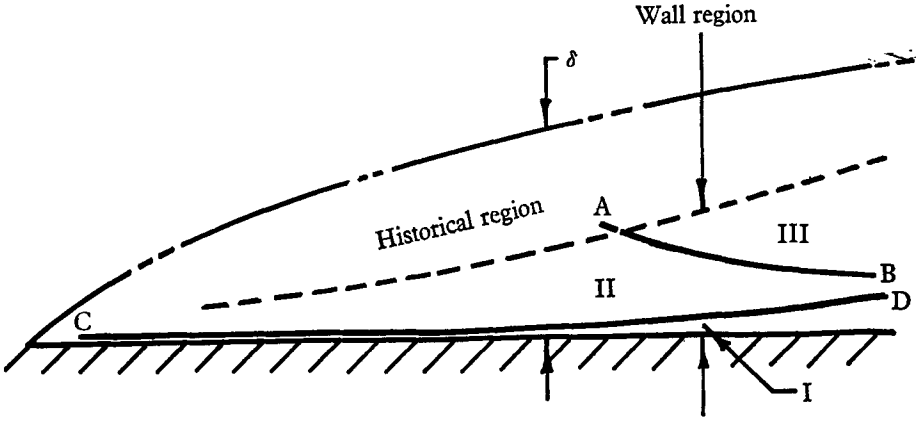

FIGURE 1. Postulated regions in an adverse pressure gradient turbulent boundary layer.

Region I

For sufficiently small values of y, α can be excluded from the analysis.

Region II

For sufficiently large values of y, mean relative motions will be independent of ν. However, y is not sufficiently large for α to have an influence.

Region III

For sufficiently large values of y, mean relative motions are independent of ν and also of the wall shear stress τ_0, provided the boundary layer has developed sufficiently.† This possibility will be allowed for in the analysis, even though the local shear stress τ at a point in region III may still be of the same order as τ_0.

Analytical deductions

These assumptions lead to the following.

For region I

$$U/U_\tau = f(yU_\tau/\nu), \tag{2}$$

where $U_\tau = (\tau_0/\rho)^{\frac{1}{2}}$, and is the shear velocity.

For region II, the familiar logarithmic law of the wall is obtained, viz.

$$\frac{U}{U_\tau} = \frac{1}{\kappa}\ln\left(\frac{yU_\tau}{\nu}\right) + A, \tag{3}$$

where κ and A are universal constants.

† This has been used by the authors for the want of a more specific criterion.

For region III, the assumptions stated earlier imply that gradients of velocity are given by

$$\partial U/\partial y = f_1(\alpha, \rho \text{ and } y \text{ alone}),$$

since these are the only wall variables left when τ_0 and ν are eliminated. Dimensional analysis yields

$$\partial U/\partial y = K'\alpha^{\frac{1}{2}}y^{-\frac{1}{2}},$$

where K' is a universal constant.

Integration gives

$$U = K(\alpha y)^{\frac{1}{2}} + \Delta U_1,$$

where K is equal to $2K'$ and ΔU_1 is a function of integration which is independent of y. However, from equation (1) absolute velocities must in general be dependent on all of the wall variables, i.e.

$$\frac{U}{U_\tau} = f_2\left(\frac{\alpha y}{U_\tau^2}, \frac{U_\tau^3}{\alpha\nu}\right).$$

From this equation and the two previous ones it can be seen that the velocity must be given by

$$\frac{U}{U_\tau} = K\left(\frac{\alpha y}{U_\tau^2}\right)^{\frac{1}{2}} + \frac{\Delta U_1}{U_\tau}\left(\frac{U_\tau^3}{\alpha\nu}\right). \tag{4}\dagger$$

This will be referred to as the 'half power law' and $\Delta U_1/U_\tau$ will be referred to as the 'slip function' and represents the non-dimensional velocity of slip at the wall if this equation is extrapolated to the wall.

Equations (3) and (4) apply to regions which are separated by a blending region of unknown width. If each of these equations is extrapolated into this blending region, the location y_c, of their point of intersection‡ cannot depend on ν if consistency about the relative motions in regions II and III is to be maintained.

Dimensional analysis leads to

$$y_c = NU_\tau^2/\alpha, \tag{5}$$

where N is a universal constant. The locus of y_c is shown as line AB in figure 1. The line CD represents the outer edge of the viscous region where $y = y_b$ and

$$y_b = M\nu/U_\tau, \tag{6}$$

where M is a universal constant by dimensional analysis.

Provided y_c does not come too close to the value y_b, that is, provided $U_\tau^3/\alpha\nu$ is sufficiently large, a logarithmic region will exist. Substituting equation (5) into equation (3), the velocity U_c at the point of intersection of the extrapolated logarithmic and half power laws is given as

$$\frac{U_c}{U_\tau} = \frac{1}{\kappa}\ln\left(\frac{NU_\tau^3}{\alpha\nu}\right) + A.$$

† Throughout this paper, brackets after $\Delta U_1/U_\tau$, $\Delta U_2/U_\tau$ etc., denote a functional dependence.

‡ These equations may not intersect in the blending region, in fact, they may not intersect at all. However, the end result of a modified analysis is the same as given here, but the derivation is more lengthy.

If, on the other hand, equation (5) is substituted into equation (4), U_c is given as

$$U_c/U_\tau = K(N)^{\frac{1}{2}} + (\Delta U_1/U_\tau).$$

From these two above equations it can be seen that

$$\frac{\Delta U_1}{U_\tau} = \frac{1}{\kappa}\ln\left(\frac{NU_\tau^3}{\alpha\nu}\right) + A - K(N)^{\frac{1}{2}},$$

and by regrouping the constants this may be written as

$$\frac{\Delta U_1}{U_\tau} = \frac{1}{\kappa}\ln\left(\frac{U_\tau^3}{\alpha\nu}\right) + E, \tag{7}$$

where E is a universal constant.

This may also be written as

$$\left.\begin{aligned} \frac{\Delta U_1}{U_\tau} &= \frac{1}{\kappa}\ln\left(\frac{L_e U_\tau}{\nu}\right) + A, \\ \text{where} \qquad L_e &= CU_\tau^2/\alpha. \end{aligned}\right\} \tag{8}$$

A is as in equation (3) and C is a universal constant. L_e has the dimensions of length and L_e/C is the distance from the wall at which the stress ratio $(\tau-\tau_0)/\tau_0$ is unity. However this is true only if the mean-flow inertia forces can be neglected.

As the parameter $U_\tau^3/\alpha\nu$ approaches zero, the logarithmic law completely disappears and it can be shown from dimensional reasoning that for diminishing significance of U_τ,

$$\frac{\Delta U_1}{U_\tau} = G\left(\frac{U_\tau^3}{\alpha\nu}\right)^{-\frac{1}{3}}, \tag{9}$$

where G is a universal constant.

If surface roughness is included in the problem, assuming that relative motions outside a modified boundary region I are independent of the roughness scale and ν, then dimensional reasoning gives:

Region II

$$\frac{U}{U_\tau} = \frac{1}{\kappa}\ln\left(\frac{yU_\tau}{\nu}\right) + A - \frac{\Delta U_2}{U_\tau}\left(\frac{k_e U_\tau}{\nu}\right), \tag{10}$$

where $\Delta U_2/U_\tau$ is the roughness function and k_e is the equivalent roughness scale, defined in equation (12) (see Perry & Joubert 1963).

Region III

$$\frac{U}{U_\tau} = K\left(\frac{\alpha y}{U_\tau^2}\right)^{\frac{1}{2}} + \frac{\Delta U_1}{U_\tau}\left(\frac{U_\tau^3}{\alpha\nu}\right) - \frac{\Delta U_2}{U_\tau}\left(\frac{k_e U_\tau}{\nu}\right). \tag{11}$$

However, in this case $\Delta U_1/U_\tau$ must be given by equation (8), that is, a logarithmic region of velocity profile must exist otherwise the effect of the parameters $U_\tau^3/\alpha\nu$ and $k_e U_\tau/\nu$ cannot be separated in the way shown in equation (11) by dimensional reasoning alone.

If the flow is completely rough, ν is not involved in any region and so from equation (10)

$$\frac{\Delta U_2}{U_\tau} = \frac{1}{\kappa}\ln\left(\frac{k_e U_\tau}{\nu}\right) + A, \tag{12}$$

where A is as in equation (3) by definition of k_e. For this completely rough flow, equation (11) becomes

$$\frac{U}{U_\tau} = K\left(\frac{\alpha y}{U_\tau^2}\right)^{\frac{1}{2}} + \frac{1}{\kappa}\ln\frac{L_e}{k_e}. \tag{12a}$$

Again this is valid only so long as a logarithmic region exists, that is, provided this time y_e/k_e is sufficiently large. From dimensional considerations the thickness of the boundary region for a given geometrical configuration of roughness is now proportional to k_e.

Equation (3) is the result arrived at by Millikan (1938) and Rotta (1962) who used similar reasoning to that used here.

Equations (10) and (12) were arrived at by Hama (1954) and Clauser (1954, 1956). A special form of the half-power law and equation (9) were deduced in a paper by Stratford (1959) for a layer with continually zero wall shear stress.

The form of equations (4) and (8) (the half power equation) were essentially arrived at by Townsend (1961) from energy considerations and structural similarity arguments. This led to the conclusion that an eddy-viscosity concept could be used in regions close to the wall (equilibrium layers) and that the mean relative motions of the fluid at a point are governed by the local shear stress at that point. Mean-flow inertia forces were assumed to be small, giving a linear stress layer. This resulted in an equation applicable to regions II and III which is asymptotic to the logarithmic law at low values of $\alpha y/U_\tau^2$, and asymptotic to the half-power law at fairly large values of $\alpha y/U_\tau^2$.

This equation is

$$\frac{U}{U_\tau} = \frac{1}{\kappa}\ln\left[\frac{4U_\tau^3}{\nu\alpha}\frac{\{1+(\alpha y/U_\tau^2)\}^{\frac{1}{2}}-1}{\{1+(\alpha y/U_\tau^2)\}^{\frac{1}{2}}+1}\right] + A - \frac{2(1-B)}{\kappa} + \frac{2(1-B)}{\kappa}\left(1+\frac{\alpha y}{U_\tau^2}\right)^{\frac{1}{2}},$$

where B is a diffusion coefficient associated with the spread of turbulent energy due to turbulent diffusive movements and by working against turbulent pressure gradients.

In the authors analysis, fewer assumptions are made and the resulting logarithmic law and half-power law need not necessarily be separated by a large blending region as is given in the Townsend equation.

3. Analysis of velocity profile data

The correlation scheme which has been derived here was used for examining the two-dimensional adverse pressure gradient flow data of Schubauer & Klebanoff (1950), Perry & Joubert (1963) who used a rough wall, and some recent measurements by the authors. Also the experimental results of Johnston (1957, 1960) were examined. He measured the behaviour of a turbulent boundary layer which was yawed symmetrically as it approached the end wall of a tee section in a rectangular duct, and the 'plane of symmetry' profiles are examined here. This is shown diagrammatically in figure 6.

Figure 2 shows how the two-dimensional flow velocity profiles correlate according to equations (10) and (11). A half-power scale has been used for the abscissa, giving a linear region for the half-power law.

The Schubauer & Klebanoff profile used in figure 2 was at $x = 22{\cdot}5$ ft. This was one of the profiles which showed an appreciable logarithmic region, and the wall shear stress was determined using a Clauser chart (see Clauser 1954). All other profiles in this paper were examined in a similar way.

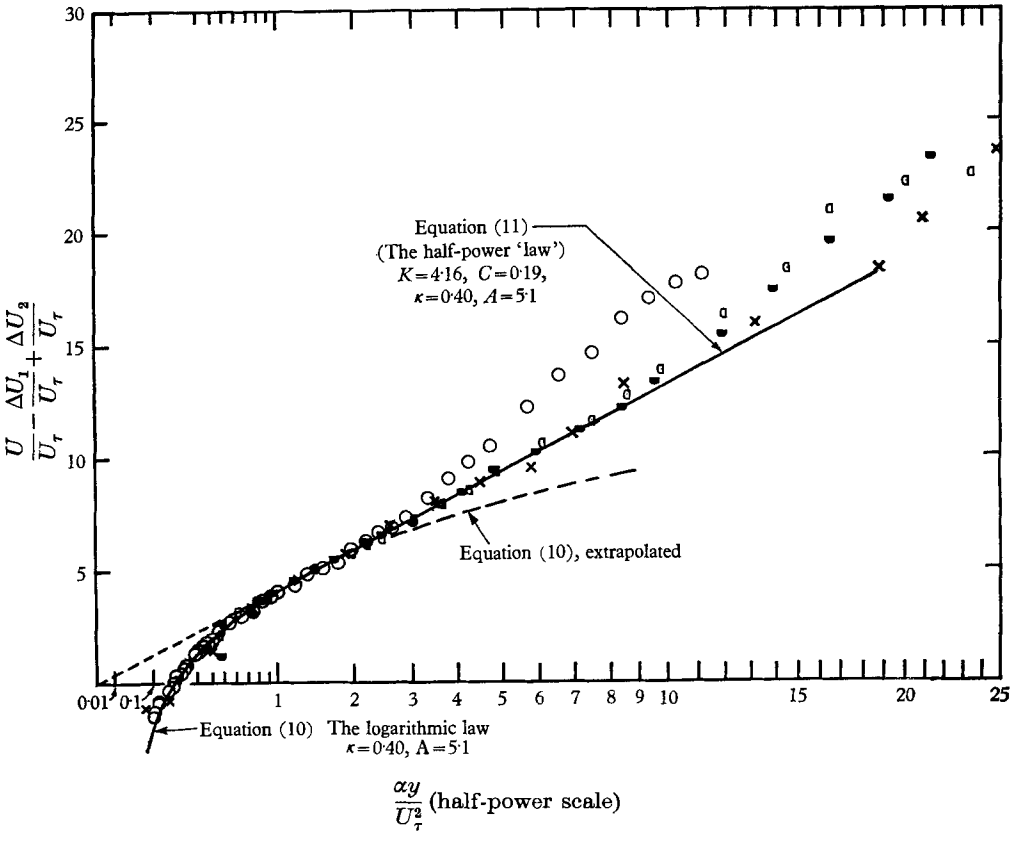

FIGURE 2. Correlations of velocity profiles. ○, Perry & Joubert (rough wall, Profile III 6); ×, Schubauer & Klebanoff (smooth wall); E 2 ●, E 5 ◁, authors (smooth wall).

Figure 3 shows the corresponding slip functions for the profiles given in figure 2, and figure 4 shows the correlation of the roughness function with equation (12) for the rough-wall profiles of Perry & Joubert and those of other sources. Also shown is the roughness geometry.

It can be seen that all experimental data appear to correlate quite well and the numerical values for the constants used are

$$\kappa = 0{\cdot}40, \quad A = 5{\cdot}1, \quad C = 0{\cdot}19 \quad \text{and} \quad K = 4{\cdot}16.$$

For this work the values of only C and K were adjustable. The values of κ and A have been well established elsewhere.

One encouraging point about the above correlation is the possibility that the mean flow inertia forces do not affect the result provided the boundary layer

is sufficiently developed. This is illustrated by examining the development of the rough-wall boundary layer of Perry & Joubert shown in figure 5.†

The last downstream profile exhibits what appears to be the start of a half-power region and yet the profile is far from separation (close to separation, inertia forces are supposedly low). Further evidence of this is shown in the development of the plane-of-symmetry profiles of Johnston shown in figure 6. A different

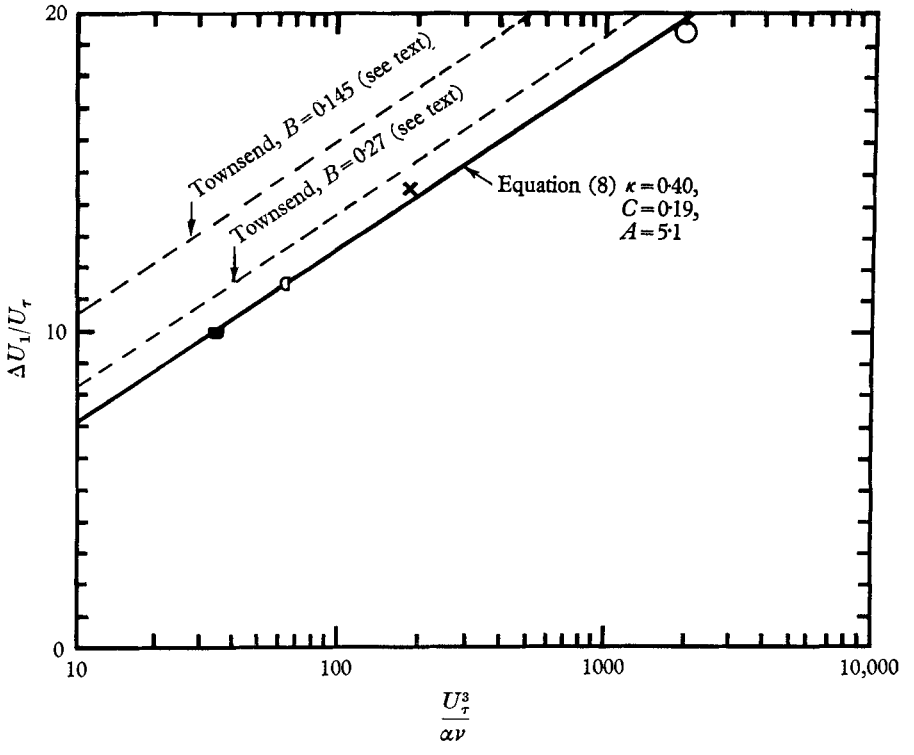

FIGURE 3. The 'slip' function. ○, Perry & Joubert (rough wall), $\Delta U_2/U_\tau = 13{\cdot}3$; ×, Schubauer & Klebanoff (smooth wall); *E* 2 ●, E 5 ◨, authors (smooth wall).

method of plotting the profiles has been used, and it can be seen that the velocity in the region of half-power correlation is quite large for some profiles, implying appreciable inertia forces.

The mean flow inertia forces present in the Perry & Joubert profiles were calculated with the aid of a plot of the wall streamlines. If these inertia forces are zero, the ratio $(\partial\tau/\partial y)/\rho\alpha$ should equal unity. This ratio is shown plotted in figure 7 for the last downstream profile. The velocity profile is also shown in this figure on a half-power plot. The major contribution to the inertia forces came from the acceleration term $U\,\partial U/\partial x$, while $V\,\partial U/\partial y$ was two orders of magnitude lower, (V is the component of velocity normal to the wall).

† The values of skin friction $5{\cdot}6(\frac{1}{2}C_f')^{\frac{1}{2}}$ of Perry & Joubert (1963) shown in table 1 of that article are quoted incorrectly for profiles III 5 and III 6. The values should be interchanged. C_f' actually varied monotonically with x as seen by the abscissae of figures 9 and 13 of the same article.

For the range of $0 < y/\delta \leqslant \frac{1}{4}$, a formula of the following form appeared adequate for the profiles examined

$$\frac{1}{\rho\alpha}\frac{\partial\tau}{\partial y} = 1 - \left(\frac{y}{L_a}\right)^{\frac{1}{2}},$$

L_a is a length scale associated with the mean flow accelerations and for the last downstream profile $L_a \approx 1{\cdot}38$ ft.

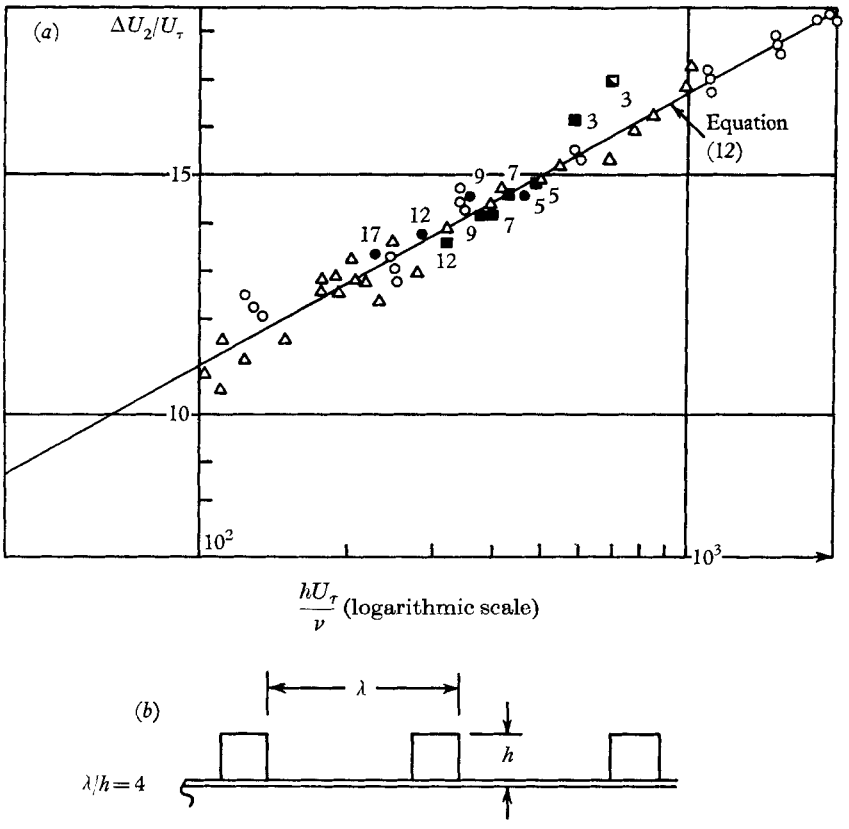

FIGURE 4(*a*). Roughness function. Numbers indicate distance in ft., from leading edge of plate. Δ, Rand, flume; ○, Moore, boundary layer with zero pressure gradient. Perry & Joubert, boundary layer with pressure gradient: ■, II series; ●, III series; ◪, II 1–1·5 ft. of plate unroughened at leading edge. (*b*) Roughness geometry applicable to figure 4(*a*).

The philosophy adopted by the authors in the similarity analysis is somewhat similar to that of Coles (1955) who assumed that the profile $U/U_\tau = f(yU_\tau/\nu)$ retained its universality irrespective of the state of balance of momentum given by the mean flow equations. The momentum equation was regarded to be irrelevant in determining the profile close to the wall (when the above similarity parameters are used) but was of importance in determining the distribution of wall shear stress and boundary-layer development. From this and the continuity

equation he deduced his streamline hypothesis and arrived at an expression for the distribution of shear stress within the 'law of the wall' This is given as

$$\frac{\tau}{\tau_0} = 1 + \frac{\alpha y}{U_\tau^2} + \frac{\nu}{U_\tau^2}\frac{dU_\tau}{dx}\int_0^{yU_\tau/\nu}\left(\frac{U}{U_\tau}\right)^2 d\left(\frac{yU_\tau}{\nu}\right).$$

For some of the tests carried out by the authors, the shear stress ratio given by the above equation was approximately 2 at the outer edge of the logarithmic layer as compared with 2·4 if the mean flow inertia forces are neglected. The above equation is not applicable in the half-power region.

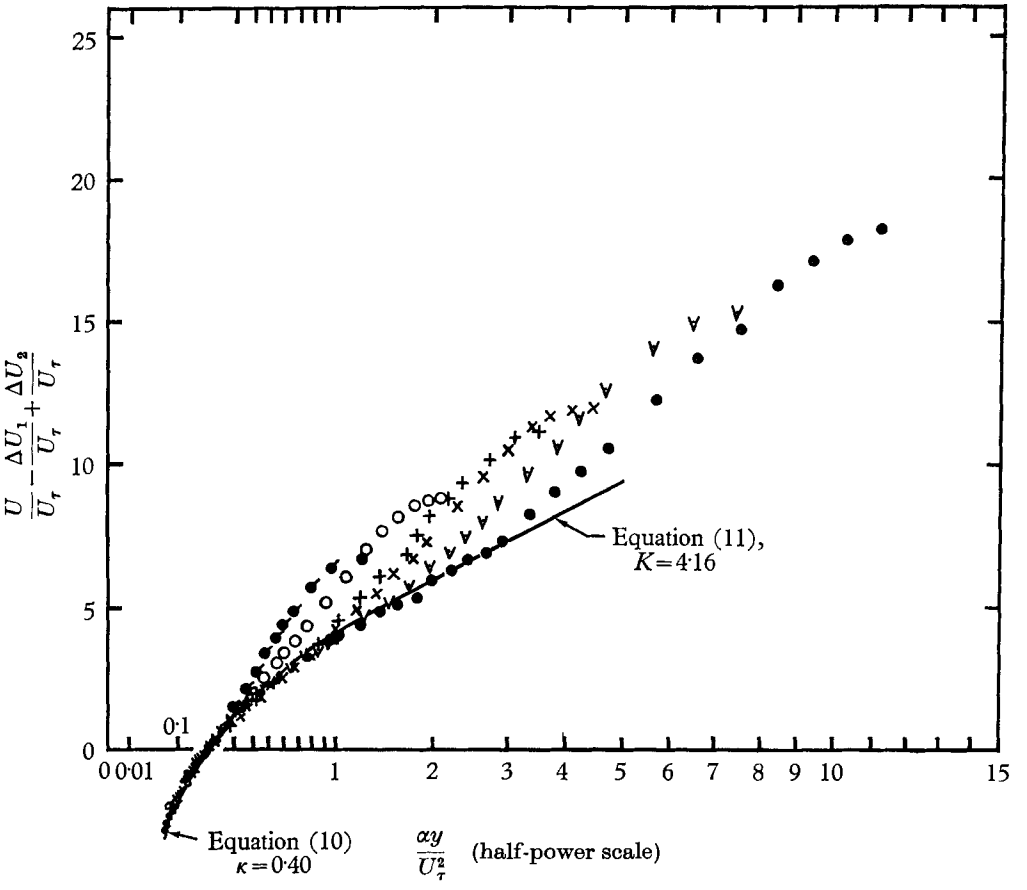

FIGURE 5. Development of a rough-wall boundary layer in an adverse pressure gradient. Profiles of Perry & Joubert (1963):

Profile	Distance x ft. from leading edge	Profile	Distance x ft. from leading edge
● III 1	3	× III 4	9
○ III 2	5	∀ III 5	12
+ III 3	7	● III 6	17

The value of K used by the authors agrees with the value used by Townsend (1961) and Stratford (1959). Townsend took into account the value of the mean flow inertia forces of Schubauer & Klebanoff and assumed that their effect was

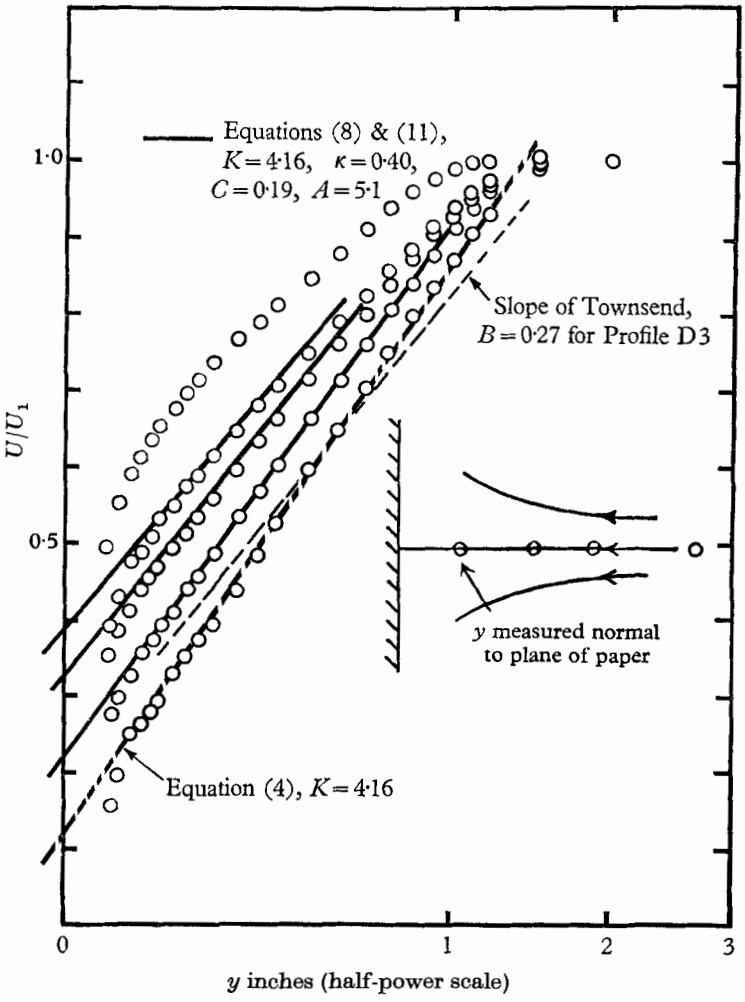

FIGURE 6. Plane of symmetry profiles of Johnston (1957, 1960). U_1 is the local free-stream velocity. In order from the top down:

	$U_\tau^3/\alpha\nu$
D 8	∞
D 4	79·3
D × 6	47·5
D × 5	21·6
D 3	8·67

to give a constant value of $(\partial\tau/\partial y)/\rho\alpha$ somewhat less than unity for a given profile. The accelerations were calculated to be approximately one-third of the kinematic pressure gradient and the resulting value of $(1/\rho)(\partial\tau/\partial y)$ was used instead of α in an equation of the form given by equation (4), since this is what the local similarity theory demanded. This agreed well with the slopes of the Schu-

bauer & Klebanoff profiles on a half-power plot. The intercepts, and hence the slip functions, were not checked, since for most profiles the values of wall shear stress were unreliable. These slopes are shown dotted in figure 8. The authors have calculated the slopes, ignoring the effect of mean flow accelerations and these are shown heavy. Both sets of lines appear to fit the data satisfactorily

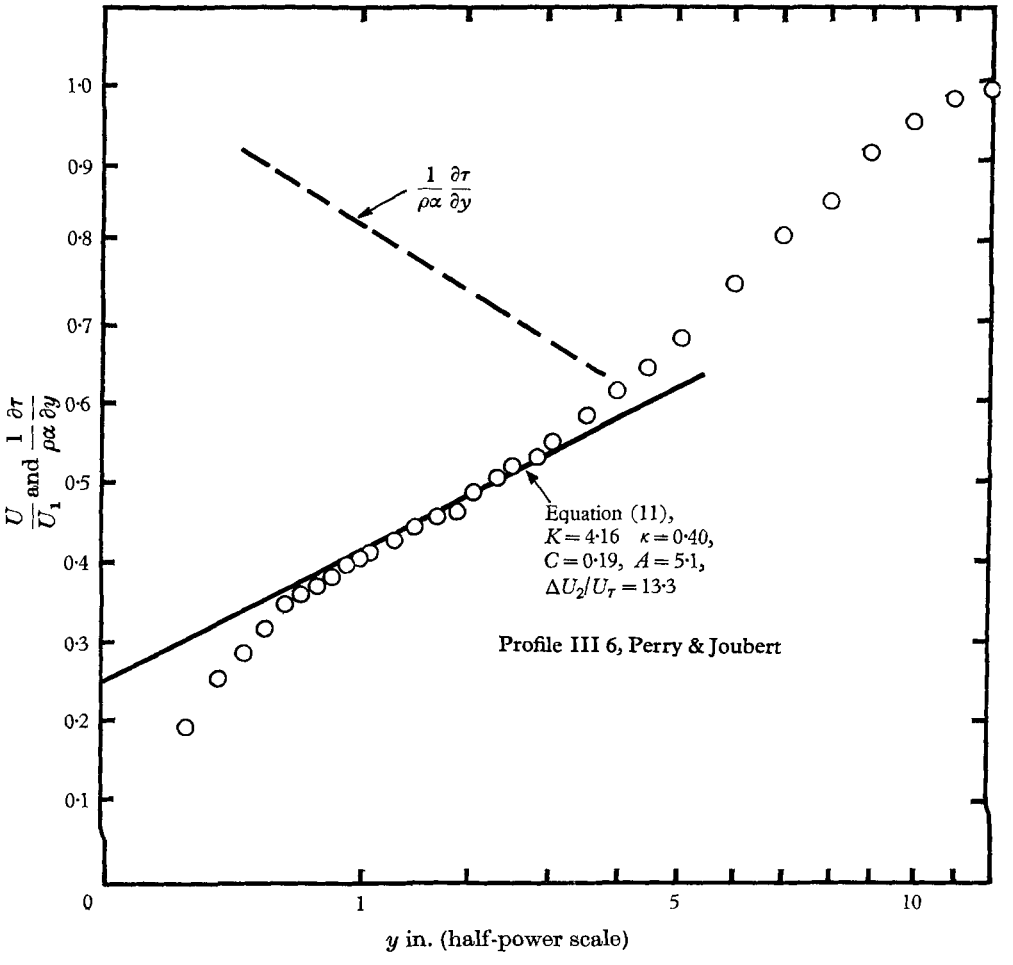

FIGURE 7. Variation of local shear stress for last downstream profile (Perry & Joubert 1963, rough wall).

provided the lines are positioned appropriately. Therefore it is possible that the inertia forces do not have an appreciable effect.

The comparison of the correlation with Townsend's theory shows a marked difference when the intercepts are considered. The local similarity theory of Townsend gives a relationship between the constants K and C which prevents the theory from fitting the data satisfactorily. The mechanism chosen appears to be too restrictive and only one adjustable constant appears. This constant is a diffusion constant B. Figure 9 shows a family of curves corresponding to

Townsend's equation for different values of B and these are compared with the authors' proposed equations.

With what appears to be the correct value of $K(= 4{\cdot}16)$, the Townsend asymptote to the half-power law has a slip function with $C = 0{\cdot}8$ and the corresponding value of B is 0·145. The authors have used $C = 0{\cdot}19$ and the comparison can be

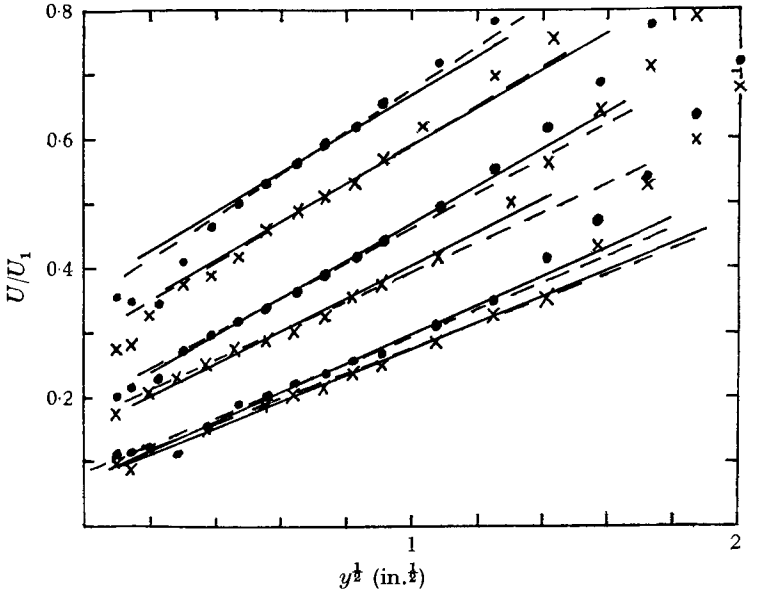

FIGURE 8. Velocity profiles of Schubauer & Klebanoff (1950). Profiles from the top to bottom are at $x = 22$, 23, 24, 24·5, 25 and 25·4 ft. respectively. Reynolds number = 10^6 ft.$^{-1}$. Dashed lines represent Townsend's calculations. Heavy lines represent authors' calculations with inertia forces neglected.

seen in figure 3. As the value of B is increased, the resulting slip function comes closer to the experimental results but the value of K is decreased. This can be seen in figure 9.

This reduced value of K definitely disagrees with the slopes of the 'near to separation' profiles of Schubauer & Klebanoff or those of Johnston (e.g. see figure 6). The authors have tested this point with Stratford's profiles. However, the profiles when plotted in the form used by the authors, are too scattered to be conclusive.

Compared with other analyses, fewer commitments about the nature of the flow processes have been made in this paper and this means that one more disposable constant is available which enables the data to be correlated more easily. Hence the authors wish to emphasize that the validity of the half-power expression derived here must rest heavily on experimental justification over a wide range of observations. This is also true of the logarithmic law deduced by Millikan, since this law, like the half-power expression, has two disposable constants.

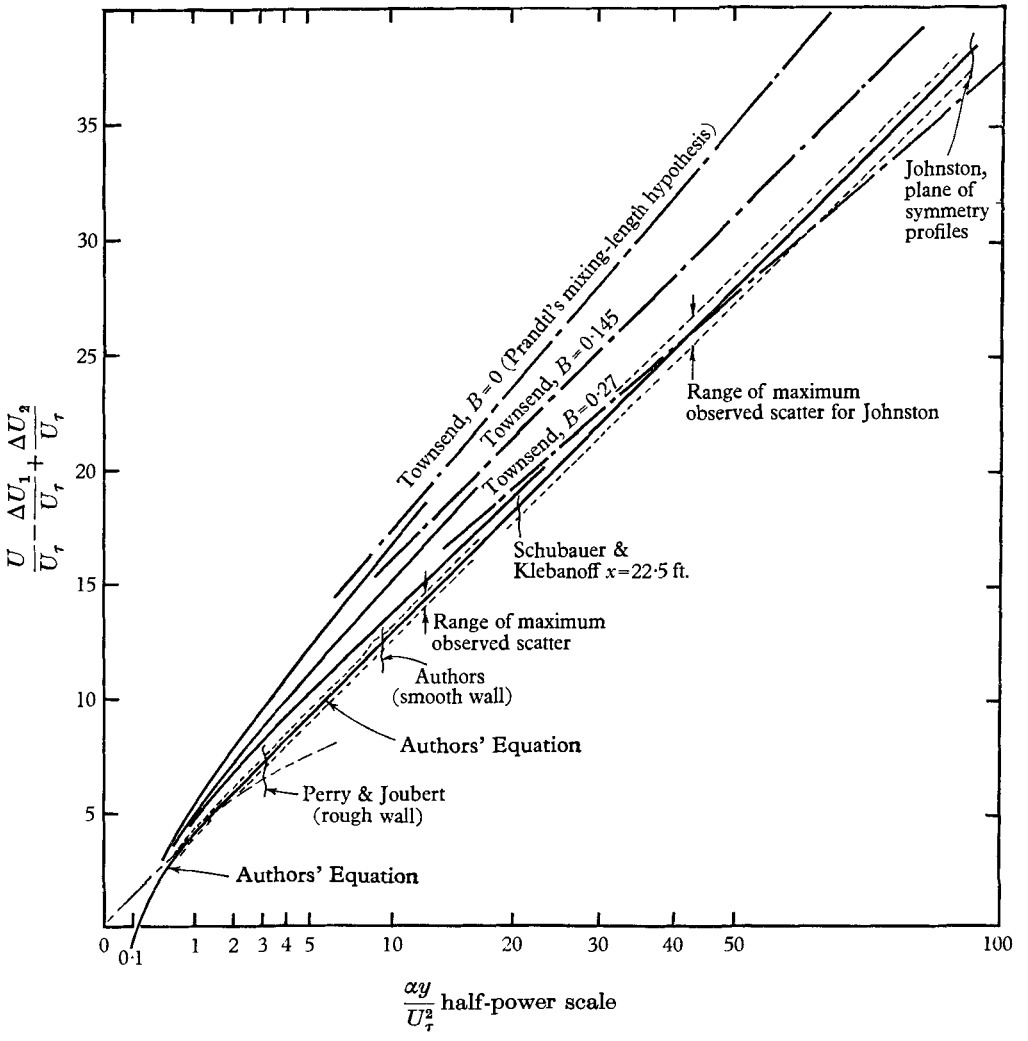

FIGURE 9. Comparison of Townsend's theory with authors' proposed equations. Townsend's theory is shown for various values of the diffusion coefficient B. The range of experimental scatter is shown and the range of $\alpha y/U_\tau^2$ for various sources is indicated by the vertical wavy lines. Townsend's equation with $B = 0{\cdot}27$ is within the experimental scatter for fairly large $\alpha y/U_\tau^2$. However, when individual profiles are considered, the trends of results do not agree (e.g. see figure 6).

4. Physical implications

The above results cast some doubts on the assumption that momentum transport depends on the local gradient-type diffusion mechanism generally used, since this requires a large blending region between the logarithmic and half-power region. With the numerical constants used by the authors, it is found that the half-power law joins onto the logarithmic law almost tangentially without any obvious blending region. This occurs at a value of $\alpha y/U_\tau^2 = 1{\cdot}41$.

It appears that the local kinematic pressure gradient does not distort the logarithmic profile but simply controls its range of application of y for a given

wall shear velocity. It is as if the flow is dominated by one effect at a time, these effects occurring in regions.

In the local similarity theory, as opposed to what could be termed the 'regional similarity hypothesis', the local velocity gradients are influenced by the local shear stress which for zero mean flow inertia forces is given by

$$\frac{\tau}{\rho} = \frac{\tau_0}{\rho} + \alpha y.$$

As αy becomes large, τ_0/ρ can be seen to become unimportant, this giving the half-power law. However, the experimental data appear to give half-power laws when αy is only 1·41 times the value of τ_0/ρ. The local similarity theory also implies that a half-power law is applicable only to layers close to separation. It has been shown here that the range of application is probably wider.

5. Criterion for the existence of a logarithmic velocity distribution

Taking the outer edge of region *I* as being $yU_\tau/\nu = 30$ and the connexion between the regions II and III occurring at $\alpha y/U_\tau^2 = 1{\cdot}41$, then so long as $U_\tau^3/\alpha\nu$ is larger than 20, a logarithmic law should exist (compare with Townsend who used $U_\tau^3/\alpha\nu \gg 20$). The last downstream profile of Johnston has a value of $U_\tau^3/\alpha\nu$ of about 8·7† (see figure 6) and no sensible logarithmic region exists. The slip function is therefore not given by equation (8). However, the slope of the half-power region of the profile agrees quite well with the value of 4·16 for K.

6. Analysis of temperature profiles

Assumptions

Close to the wall there will be a region where only the wall variables govern the flow and heat transfer. That is, the difference θ in wall and fluid mean temperature is given by

$$\theta = f(y, \rho, \nu, \tau_0, \alpha, q_0, c_p, k, k_e),$$

where c_p is the specific heat of the fluid, k is the thermal conductivity, and q_0 is the wall heat flux.

Flow will be considered to be incompressible and the fluid-property variations small. Also the amount of heat being conveyed from the wall will be considered large compared with the heat produced by viscous dissipation (i.e. low Eckert number). Therefore five fundamental quantities may be used in the dimensional analysis. As far as the effects of τ_0 and α are concerned, three regions similar to those considered earlier for the relative motions will be assumed applicable here for the relative temperatures. However, the ranges occupied by these regions need not necessarily be the same as those of the velocity profiles. In order to make analytical deductions of the type given earlier for the velocity profiles and still retain the possible effect of Prandtl number in the fully turbulent part of the flow outside the boundary region I, it is necessary to assume that the relative temperatures $\partial\theta/\partial y$ are independent of the length scales associated with this boundary region. Such length scales are ν/U_τ (proportional to the thick-

† The value of τ_0/ρ was guessed for this case by noting the position of the points close to the wall on a Clauser chart.

ness of the viscous sublayer) and $k/\rho c_p U_\tau$ (proportional to the thickness of the thermal conduction sublayer). The relative temperatures must also be independent of k_e, the surface roughness scale.

Analytical deductions

The resulting equations are:

Region I
$$\frac{\theta}{\theta_\tau} = f\left(\frac{yU_\tau}{\nu}, \sigma, \frac{k_e U_\tau}{\nu}\right), \tag{13}$$

where θ_τ is the friction temperature equal to $q_0/(\rho c_p U_\tau)$ and σ is the Prandtl number.

Region II
$$\frac{\theta}{\theta_\tau} = \frac{1}{\kappa_H(\sigma)} \ln\left(\frac{yU_\tau}{\nu}\right) + A_H(\sigma) - \frac{\Delta\theta_2}{\theta_\tau}\left(\sigma, \frac{k_e U_\tau}{\nu}\right). \tag{14}$$

Region III
$$\frac{\theta}{\theta_\tau} = K_H(\sigma)\left(\frac{\alpha y}{U_\tau^2}\right)^{-\frac{1}{2}} + \frac{\Delta\theta_1}{\theta_\tau}\left(\frac{U_\tau^3}{\alpha\nu}, \sigma\right) - \frac{\Delta\theta_2}{\theta_\tau}\left(\sigma, \frac{k_e U_\tau}{\nu}\right). \tag{15}$$

The quantities κ_H, K_H and A_H are analogous to the universal constants κ, K and A used in the description of the velocity profiles. However, the analysis shows that it is possible for these former quantities to be functions of Prandtl number. The usual theories of thermal transport, such as the various modified Reynolds analogies, arrive at a form similar to equation (14) with these various terms being functions of Prandtl number. However, κ_H is given as a function of Prandtl number only if the concept of a uniform turbulent Prandtl number is used in these theories. Also the shear stress and heat flux must be assumed to be invariant with y to arrive at the form of (14), whereas it is not necessary to make these assumptions here.

The functions $\Delta\theta_1/\theta_\tau$ and $\Delta\theta_2/\theta_\tau$ are somewhat analogous to the velocity slip and roughness functions. From similar reasoning to that used for the velocity distributions, the form of equation (15) is valid for the rough wall case† only so long as there is a logarithmic distribution of temperature present, and it can be deduced that
$$\frac{\Delta\theta_1}{\theta_\tau} = \frac{1}{\kappa_H(\sigma)} \ln\left(\frac{U_\tau^3}{\alpha\nu}\right) + D(\sigma). \tag{16}$$

As $U_\tau^3/\alpha\nu$ approaches zero, the effect of U_τ disappears, and this requires
$$\frac{\Delta\theta_1}{\theta_\tau} = G_H(\sigma)\left(\frac{U_\tau^3}{\alpha\nu}\right)^{\frac{1}{3}}, \tag{17}$$

provided surface-roughness effects are small. G_H is analogous to G in the velocity-profile equations.

7. Analysis of temperature profile data and description of experiment

The form of equation (14) has been verified experimentally to some extent by Reynolds, Kays & Kline (1958), who measured the temperature profiles in a zero pressure gradient turbulent boundary layer. The wall was smooth and was

† For smooth walls, the form of equation (15) should be valid irrespective of whether a logarithmic temperature region exists.

heated to a uniform temperature. Figure 10 shows these results. It can be seen that a 'thermal law of the wall' exists for zero pressure gradients and some part of the profile could be interpreted to be logarithmic.

The authors' experimental conditions and apparatus were similar to those of Reynolds, Kays & Kline, except that pressure gradient effects were included. The plate was flat and smooth and held at a uniform temperature. Also, as in the

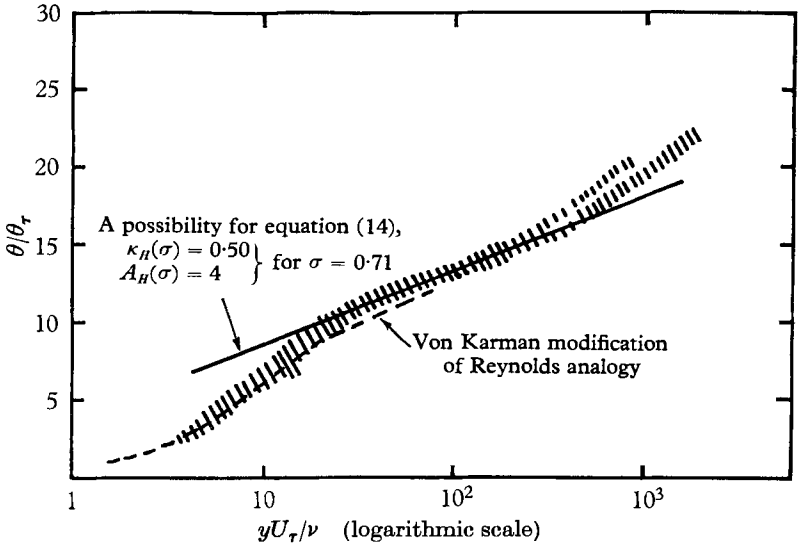

FIGURE 10. Temperature profiles of Reynolds, Kays & Kline (1958). Re_x goes from $0{\cdot}729 \times 10^6$ to $2{\cdot}78 \times 10^6$.

Reynolds, Kays & Kline tests, no appreciable unheated starting length existed. The fluid used was air, giving a Prandtl number $\sigma = 0{\cdot}71$. The maximum temperature difference between the plate and the free stream was 20 °C, giving only small variations in fluid properties. All fluid properties were evaluated at the mean viscous-zone temperature. The Eckert number was negligibly low.

Stanton numbers were measured by isolated electric heating strips. The plate was heated by low-pressure steam. Reproducibility of Stanton number was poor ($\pm 7\,\%$), and so an ensemble average was used from many repetitions of the measuring procedure. Also, faired-in curves of Stanton number plotted against many Reynolds-number values were used for each measuring station along the plate. Cursory checks were made using thermal integral methods. A detailed description of the apparatus and the correlation of experimental results of other flow cases is under preparation by the authors.

The profiles from this experiment have been plotted in the same way as those of Reynolds, Kay & Kline and are shown in figure 11. It can be seen that a thermal law of the wall, using the similarity parameters θ/θ_τ and yU_τ/ν, does not appear valid for all cases, except perhaps well within the viscous zone of the flow. Most profiles were measured only at two stations along the plate for a series of Reynolds numbers and pressure distributions.

A typical zero-pressure-gradient profile measured by the authors (No. 9) is

compared with a typical one of Reynolds, Kays & Kline, and close agreement can be seen. However, considerable departure from these occurs for some of the pressure-gradient profiles. The lower profiles labelled E 1 to E 9 were measured at a station furthermost from the leading edge (station 1). The pressure-gradient

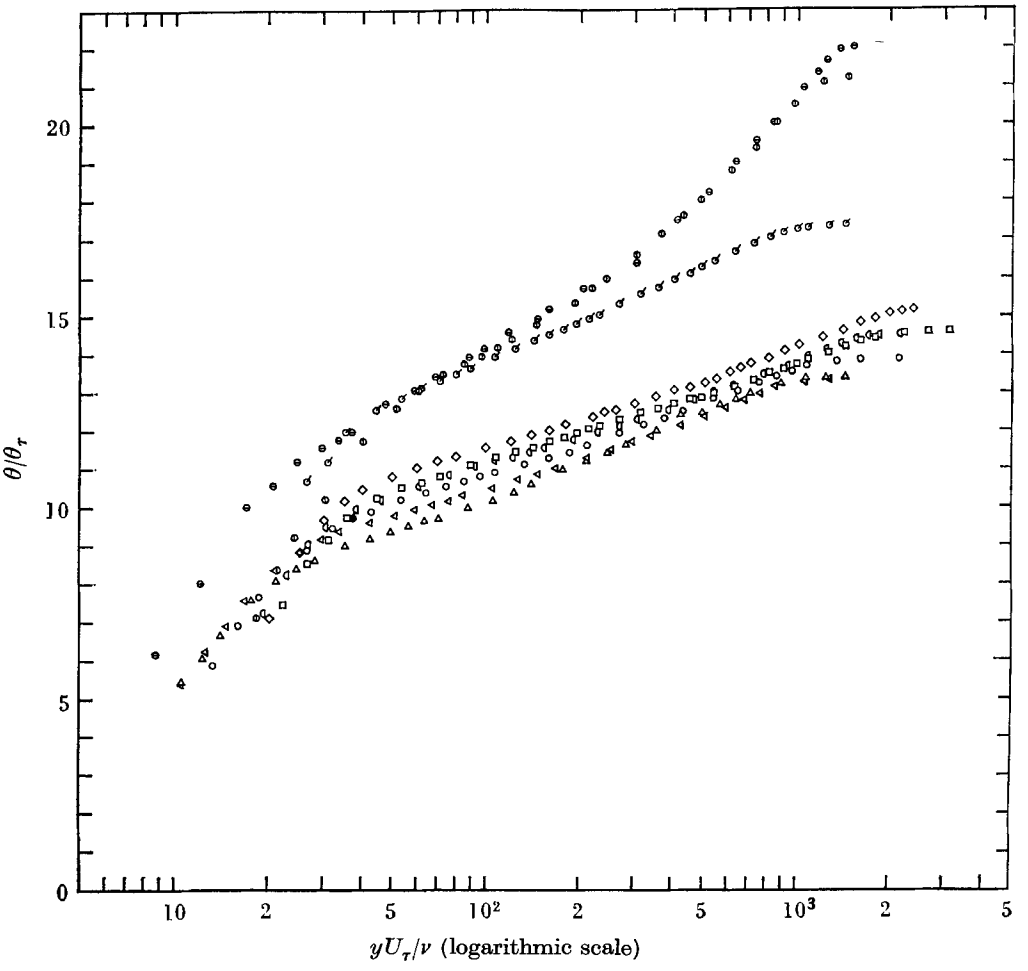

FIGURE 11. Temperature profiles of the authors. Re_x is the Reynolds number based on distance from the leading edge, C_f' is the local skin friction coefficient and St is the local Stanton number, all of which are based on the local free stream velocity.

		Re_x	C_f'	$U_\tau^3/\alpha\nu$	St
E 1	△	$0{\cdot}79 \times 10^6$	0·00134	31·8	0·00194
E 2	◁	$0{\cdot}97 \times 10^6$	0·00124	35·5	0·00188
E 3	○	$1{\cdot}21 \times 10^6$	0·00124	44·4	0·00180
E 5	◖	$1{\cdot}76 \times 10^6$	0·00124	63·9	0·00171
E 6	□	$2{\cdot}04 \times 10^6$	0·00122	73·1	0·0017
E 9	◇	$2{\cdot}26 \times 10^6$	0·0013	87·5	0·00168
E 10	⊘	$0{\cdot}926 \times 10^6$	0·0020	106	0·0018
No. 9	⊕	$1{\cdot}80 \times 10^6$	0·0030	∞	0·0018
Reynolds *et al.* (1958)	⊖	$1{\cdot}72 \times 10^6$	0·0033	∞	0·0019

profile E 10 shown, was measured halfway along the plate (station 2) and it agrees reasonably well with the Reynolds, Kays & Kline 'wall result.' The pressure distribution used for these E profiles is shown in figure 14.

Although the profiles in figure 11 depart from the zero-pressure-gradient case, they still appear to be logarithmic. This could be partially explained by a Rey-

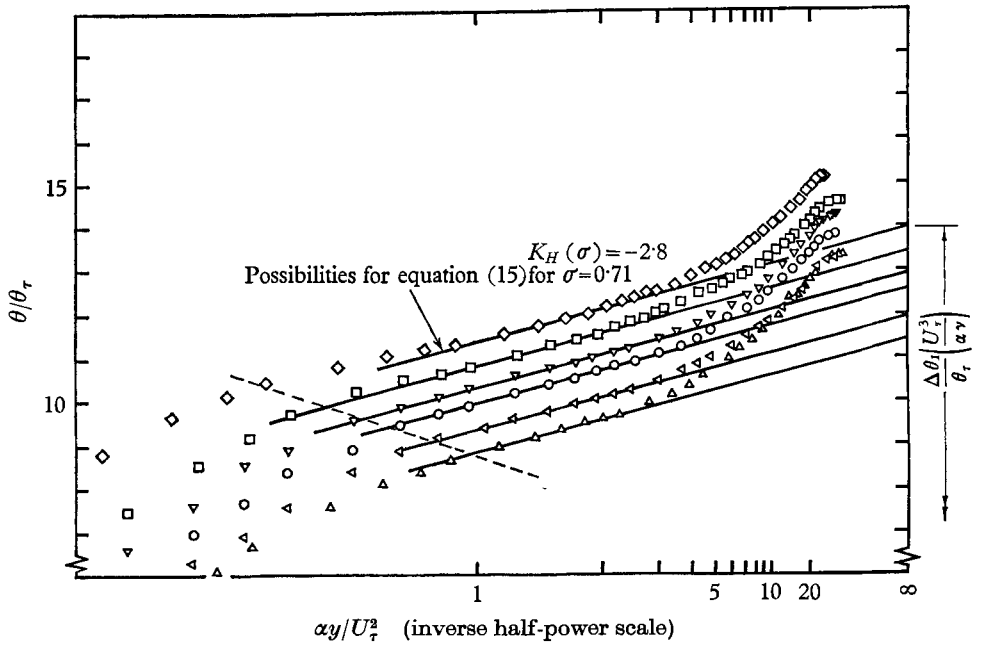

FIGURE 12. Temperature profiles plotted according to equation (15). The dashed line corresponds to $yU_\tau/\nu \approx 30$. Authors' values: ◇, E 9; □, E 6; ▽, E 4; ○, E 3; ◁, E 2; △, E 1.

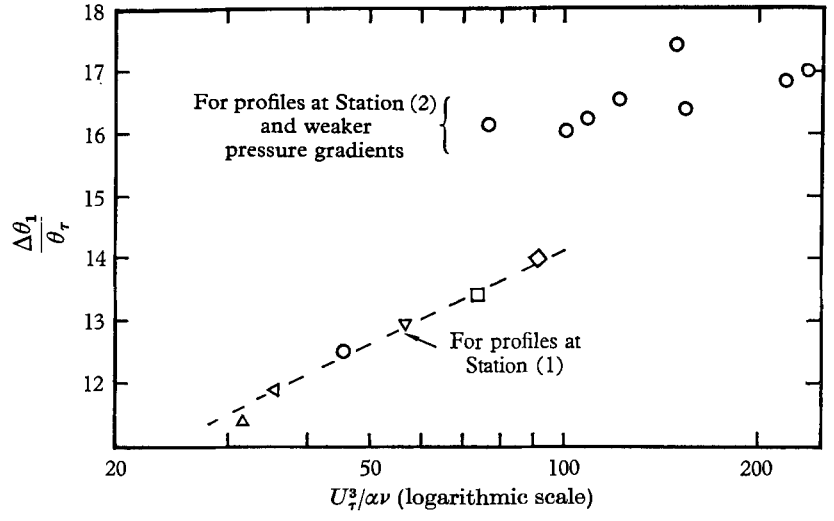

FIGURE 13. Possible correlation of the function $\Delta\theta_1/\theta_\tau$ for profiles shown in figure (12). Authors' values: △, E 1; ◁, E 2; ○, E 3; ▽, E 4; □, E 6; ◇, E 9.

nolds analogy type of analysis with the inclusion of a turbulent Prandtl number which is dependent on the pressure gradient and perhaps boundary-layer history. As opposed to this, one could include the possibility that there still exists a wall region in the sense used in the regional similarity analysis, but the effect of the local kinematic pressure gradient extends deeper into the 'thermal layer' than

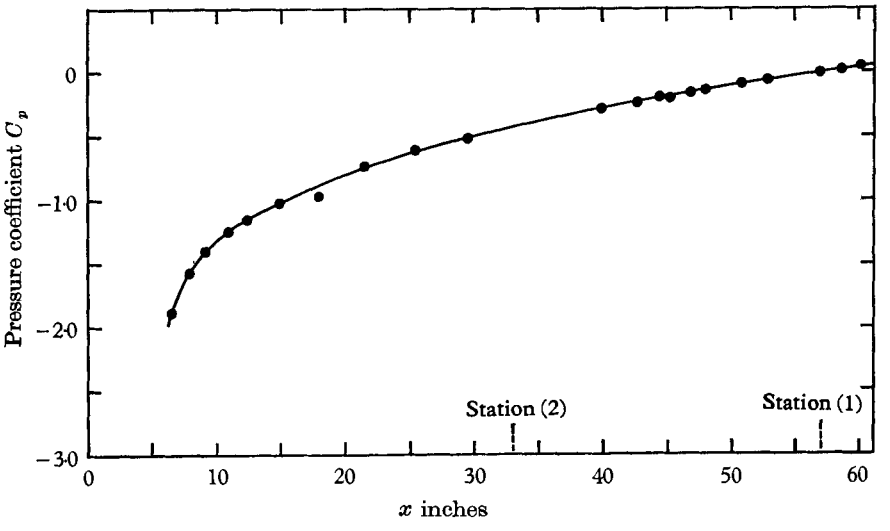

FIGURE 14. Pressure distribution for authors' E profiles. Pressure coefficients C_p is based on free stream velocity at station (1).

it does into the 'velocity layer'. The profiles (which appear to be logarithmic), correlate quite well when plotted according to equation (15), and extensive linear regions can be seen on the inverse half-power plot. These are shown in figure 12 and, in most cases, the linear regions extend down to the viscous zone, $(yU_\tau/\nu \approx 30)$. The viscous-zone boundary is shown as a broken line in this figure. For these profiles then, perhaps no logarithmic region really exists.

Using this correlation, the function $\Delta\theta_1/\theta_\tau$ was plotted according to equation (15) and is shown in figure 13. For the profiles measured at station 1, the experimental points appear to fall on one unique line or curve, i.e.

$$\frac{\Delta\theta_1}{\theta_\tau} = \frac{\Delta\theta_1}{\theta_\tau}\left(\frac{U_\tau^3}{\alpha\nu}\right)$$

for the constant Prandtl number used. On first sight, one is tempted to describe this correlation by equation (16) since the value of $\kappa_H(\sigma)$ found is close to the Reynolds, Kays & Kline value seen in figure 10. However, since it is probable that no logarithmic region exists, the points may be falling on some transition function which joins equation (16) to equation (17).

The scattered points shown in figure 13 belong to profiles measured at station 2, which is closer to the leading edge (see figure 14). Also a few of these points belong to weaker pressure-gradient tests. It is conjectured that the inverse half-power equation is not applicable for these profiles, even though straight lines could be fitted to them over some region on the inverse half-power plot.

The corresponding velocity profiles failed to exhibit a half-power region and so were probably not sufficiently developed to exclude the effects of mean flow acceleration and boundary-layer history. By analogy, they may not have been sufficiently developed to exclude the effects of mean thermal convection and history. On the other hand, half-power regions were observed for the velocity profiles at station (1) for the pressure gradient shown in figure 14, and two typical ones were shown earlier in the paper (see figure 2).

These results are at least encouraging and some tentative values for the various 'constants' are

$$K_H(\sigma) \approx -2{\cdot}8, \quad \kappa_H(\sigma) \approx 0{\cdot}50, \quad \text{and} \quad A_H(\sigma) \approx 4 \quad \text{for} \quad \sigma = 0{\cdot}71.$$

8. Conclusions

It appears that for adverse pressure-gradient turbulent boundary layers which have developed sufficiently, there will exist a region close to the wall with a velocity profile which is logarithmic for small values of y and of a half-power form for larger values. The blending region between these laws is small and the resulting expressions are valid for smooth and possibly for rough walls. The theory appears to be valid for profiles much further from separation than was thought probable when using Townsend's theory. The results cast doubts on the usual local similarity concepts.

Temperature profiles appear to follow a similar correlation to the above except that an inverse half-power equation is involved.

If these correlations are verified by further experiment, they should form a good basis for an integral-type analysis for predicting the distribution of Stanton number in an adverse pressure gradient. The resulting thermal and momentum thicknesses using this velocity- and temperature-profile correlation should be quite accurate because of the reasonably large depth of profile described. However, the problem will not be completely solved until the outer region of the profiles is correlated.

The authors are indebted to the Australian Institute of Nuclear Science and Engineering for financial support of this project.

REFERENCES

CLAUSER, F. H. 1954 *J. Aero. Sci.* **21**, 19.

CLAUSER, F. H. 1956 *Advan. Appl. Mech.* **4**, 1.

COLES, D. 1955 50 *Jahre Grenzschichtforschung* (50 Years of Boundary Layer Research); eds. H. H. Goertler and W. Tollmien. Braunschweig: Friedr. Viewey und Sohn.

HAMA, F. R. 1954 *Trans. Soc. Naval Arch. Mar. Engrs.*, **62**, 333.

JOHNSTON, J. P. 1957 Three dimensional turbulent boundary layer. Sc.D. Thesis, Massachusetts Institute of Technology.

JOHNSTON, J. P. 1960 *Trans. A.S.M.E.* Series D, **82**, 233.

KESTIN, J. & RICHARDSON, P. D. 1963 *Int. J. Heat & Mass. Transfer*, **6**, 147.

MILLIKAN, C. D. 1938 *Proc. 5th Int. Congr. Appl. Mech.* pp. 386–92.

PERRY, A. E. & JOUBERT, P. N. 1963 *J. Fluid Mech.* **17**, 193.

REYNOLDS, W. C., KAYS, W. M. & KLINE, S. J. 1958 *NASA Memo.* 12-1-58 W.

ROTTA, J. C. 1962 *Progr. Aero. Sci.* **2**, 5-219.

ROTTA, J. C. 1964 *Int. J. Heat & Mass Transfer*, **7**, 216.

SCHUBAUER, C. B. & KLEBANOFF, P. S. 1950 *NACA TN* no. 2133.

SPALDING, D. B. 1961 International development in heat transfer. *ASME Inst. Mech. Eng.* **2**, 439.

STRATFORD, B. S. 1959 *J. Fluid Mech.* **5**, 1 and 17.

TOWNSEND, A. A. 1961 *J. Fluid Mech.* **11**, 97.